Volume 8 | Number 17 | 7 May 2017 | Pages 2573–2734

Polymer Chemistry

rsc.li/polymers

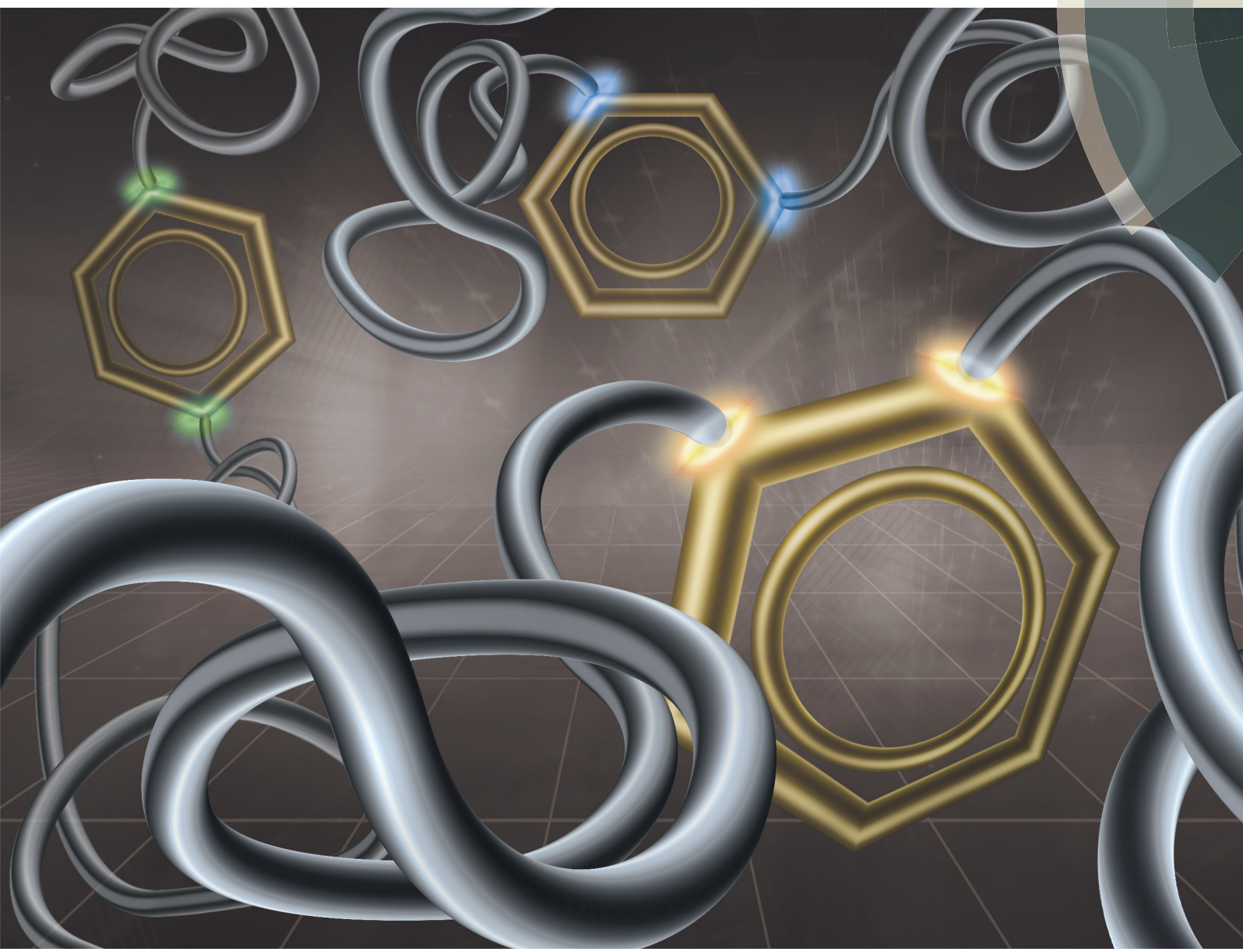

ISSN 1759-9962

ROYAL SOCIETY OF CHEMISTRY

PAPER

Lin Yu *et al.*

Positional isomeric effects of coupling agents on the temperature-induced gelation of triblock copolymer aqueous solutions

Polymer Chemistry

PAPER

View Article Online
View Journal | View Issue

Check for updates

Cite this: *Polym. Chem.*, 2017, **8**, 2586

Positional isomeric effects of coupling agents on the temperature-induced gelation of triblock copolymer aqueous solutions†

Jiabin Luan, Shuquan Cui, Juntao Wang, Wenjia Shen, Lin Yu* and Jiandong Ding

Received 12th February 2017,
Accepted 10th March 2017

DOI: 10.1039/c7py00232g

rsc.li/polymers

While the importance of molecular linkers to design functional polymers and adjust their performance has been acknowledged, their role in thermogelling polymers is still unclear. Herein, we demonstrate that the di-functional positional isomers as the coupling agents in the middle of polymer chains greatly affect the microscopic conformation and macroscopic properties of thermogelling polymers. To enable such an examination, we synthesized BAB-type triblock copolymers methoxy poly(ethylene glycol)-*b*-poly(D,L-lactic acid-*co*-glycolic acid)-*b*-methoxy poly(ethylene glycol) (mPEG-PLGA-mPEG) linking with different coupling agents. All the polymers were soluble in water at ambient temperature and the polymer solutions underwent a sol–gel transition upon heating. After replacing hexamethylene diisocyanate (HMDI), a conventional coupling agent, with positional isomers of phthaloyl dichloride (*o*-PC, *m*-PC and *p*-PC), the polymer/water system exhibited lower sol–gel transition temperatures and larger gel moduli due to the phenyl rigidity of PC. We revealed that the polymer coupled with *o*-PC had a smaller coil size owing to its 60° linkage. This spatial conformation difference further resulted in a reduced thermal gelation temperature and an increased gel modulus of the polymer/water system compared with the copolymers linking with *m*-PC and *p*-PC isomers. In addition, the formation of a percolated micelle network *via* micellar aggregation was responsible for their sol–gel transitions with increasing temperature. The present work offers more insight into the relationship between the molecular structure of polymer chains and the thermogelation behaviors of polymer aqueous solutions.

Published on 13 March 2017. Downloaded by Fudan University on 11/11/2017 01:43:32.

Introduction

Stimuli-responsive polymers and their underlying transition mechanism have been extensively investigated in polymer and materials science for the past few decades.[1–8] In particular, thermogelling polymers that undergo a thermo-reversible sol–gel transition in water have drawn much attention owing to their unique thermogelation behavior[9–14] as well as their potential biomedical applications, such as drug delivery,[15–17] tissue engineering,[18–20] post-operative anti-adhesion treatments,[21–23] submucosal injection,[24] three-dimensional cell culture,[25–27] and so on.[28] Generally speaking, temperature-induced gelation of polymer aqueous solutions originates from a delicate balance of the hydrophilicity and hydrophobicity of the polymers. To date, a variety of thermogelling polymers have been explored based on biocompatible poly(ethylene glycol) (PEG) as the hydrophilic segment and biodegradable polyesters,[16,17,19,23] polypeptides[18,20] and polyphosphazenes[29,30] as the hydrophobic blocks.

Among them, thermogelling PEG/polyester block copolymers are among the most promising candidates for use as injectable biomaterials because of their facile synthesis and good biocompatibility. Their sol–gel transition and degradation rate can be modulated *via* many molecular parameters, such as the molecular weight (MW) of blocks,[31,32] the MW distribution of polymers,[33,34] and the composition of polyester segments.[31,35,36] On the other hand, the architecture and topology of a polymer also have significant effects on the thermogelling properties.[10,37,38] For example, linear ABA-type and BAB-type triblock copolymers, where A is the hydrophobic polyester block and B is the hydrophilic PEG block, are the most common architectures for thermogelling PEG/polyester block copolymers. Compared with BAB-type copolymers, ABA-type ones exhibited a lower sol–gel transition temperature, a smaller critical gel concentration but a higher gel modulus in the case of similar total MWs and molar ratios of PEG/polyester.[38] Meanwhile, these ABA-type triblock copolymers suffered from a subtle end-group effect which is able to signifi-

State Key Laboratory of Molecular Engineering of Polymers, Department of Macromolecular Science, Fudan University, Shanghai 200433, China. E-mail: yu_lin@fudan.edu.cn; Fax: +86-21-65640293; Tel: +86-21-65642531

†Electronic supplementary information (ESI) available: Details of experiment and characterization. See DOI: 10.1039/c7py00232g

This journal is © The Royal Society of Chemistry 2017

Published on 13 March 2017. Downloaded by Fudan University on 11/11/2017 01:43:32.

cantly affect their macroscopic gelation behavior in water.[32,39–42]

In general, while ABA-type triblock copolymers were synthesized *via* one-step ring-opening polymerization of monomers using PEG with two hydroxyl end groups as the macroinitiator,[23,31,32] BAB-type triblock copolymers were prepared based on two steps: firstly, ring-opening polymerization of monomers with methoxy poly(ethylene glycol) (mPEG) to obtain BA-type diblock copolymers; secondly, the coupling of the diblock copolymers using a linking moiety to form the desired BAB-type triblock copolymers.[43,44] So far, hexamethylene diisocyanate (HMDI) has been the most common coupling agent due to its high conjugation efficiency.[43,44] In fact, linking molecules containing two functional groups can be designed as coupling agents; however, the use of other coupling agents to construct thermogelling BAB-type PEG/polyester triblock copolymers has been surprisingly quite scarce. Consequently, the impact of the type of coupling agent embedded in the middle of triblock copolymers on the micellization and thermal gelation of copolymer aqueous solutions has not been paid sufficient attention so far, and the relationship between the structural features of the coupling agents and the properties of the thermogelling polymers produced is still unclear.

In the present study, a series of thermogelling BAB-type methoxy poly(ethylene glycol)-*b*-poly(D,L-lactic acid-*co*-glycolic acid)-*b*-methoxy poly(ethylene glycol) (mPEG-PLGA-mPEG) triblock copolymers were synthesized using the different positional isomers of phthaloyl dichloride (*o*-PC, *m*-PC and *p*-PC) as the coupling agents for the first time. Their concentrated polymer aqueous solutions were free-flowing sols at room temperature and transformed into semi-solid thermogels upon heating, as presented in Fig. 1A. Meanwhile, the conventional mPEG-PLGA-mPEG triblock copolymer as the control was also prepared using HMDI. Compared with PC isomers, HMDI is more flexible. The influence of different spatial conformations of the embedded coupling agents on the microscopic structures and macroscopic properties of BAB-type triblock copolymers was systemically examined and compared using gel permeation chromatography, nuclear magnetic resonance, multi-angle light scattering, dynamic mechanical analysis, dynamic light scattering and transmission electron microscopy. The spatial conformation difference in the resulting polymers was further confirmed by a Monte Carlo simulation. Finally, the sol–gel transition mechanism was suggested and the internal structures of micelles with different positional isomers were discussed as well. The basic idea of the current study is schematically displayed in Fig. 1B.

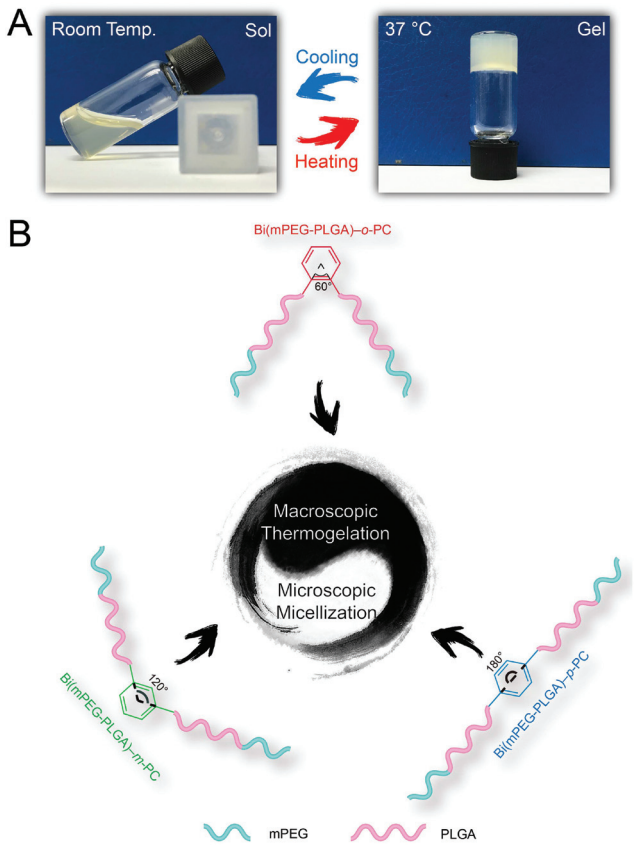

Fig. 1 (A) Photographs of the polymer aqueous solution (25 wt%) exhibiting a sol at room temperature and a gel after being heated to physiological temperature. (B) Schematic diagram showing the positional isomeric effects of PC coupling agents on the microscopic and macroscopic properties of Bi(mPEG-PLGA)–PC triblock copolymers in water. The actual conformation of the mPEG-PLGA segment is a random coil, as seen from our computer simulation in Fig. 4.

Experimental

Materials

Methoxy poly(ethylene glycol) (mPEG) with a molecular weight (MW) of ~550 g mol^{-1}, stannous octoate ($Sn(Oct)_2$, 92.5–100%), and hexamethylene diisocyanate (HMDI, 99%) were provided by Sigma-Aldrich (USA). D,L-Lactide (LA) and glycolide (GA) were purchased from Jinan Daigang Biomaterial Co., Ltd (China). Phthaloyl dichloride (*o*-PC, 98%), isophthaloyl dichloride (*m*-PC, 99%) and terephthaloyl dichloride (*p*-PC, 99%) were products of Tokyo Chemical Industry Co., Ltd (Japan). Other chemicals were of reagent grade and used as received.

Synthesis of the mPEG-PLGA diblock copolymer

mPEG-PLGA diblock copolymer was synthesized *via* ring-opening polymerization of LA and GA in the presence of mPEG as the macroinitiator. Briefly, mPEG (27.7 g) was dried in a three-neck flask at 120 °C for 3 h under vacuum. Then, LA (45.7 g) and GA (12.3 g) were added and heated at 90 °C for 30 min under reduced pressure. After adding the catalyst $Sn(Oct)_2$ (90 mg) to the reaction mixture, the system was maintained at 150 °C for 12 h with continuous stirring. Crude products were then dissolved in dichloromethane and precipitated in cold diethyl ether. The final products were collected

Published on 13 March 2017. Downloaded by Fudan University on 11/11/2017 01:43:32.

and the residual solvent in the polymers was removed under vacuum for 48 h (yield: 76%).

Synthesis of the Bi(mPEG-PLGA)–HMDI triblock copolymer

The conventional Bi(mPEG-PLGA)–HMDI triblock copolymer was prepared by coupling mPEG-PLGA with HMDI. In brief, mPEG-PLGA (7.48 g) was dissolved in 60 mL of toluene and the solvent was distilled off to a final volume of 25 mL to eliminate the residual moisture in the polymers. Then, HMDI (0.36 g) as the coupling agent and $Sn(Oct)_2$ (30 mg) as the catalyst were added into the polymer solution and the reaction system was stirred at 60 °C for 6 h. Finally, the products were precipitated using diethyl ether and dried under vacuum (yield: 84%).

Synthesis of Bi(mPEG-PLGA)–PC triblock copolymers

Bi(mPEG-PLGA)–PC triblock copolymers were synthesized through the alcoholysis of acyl chloride. For example, to synthesize Bi(mPEG-PLGA)–*m*-PC, mPEG-PLGA (5.42 g) was firstly dehydrated using the above-mentioned procedure. Then, the polymers were re-dissolved in anhydrous THF after removing the toluene and Et_3N (0.85 g) was added. Next, the solution of *m*-PC (0.31 g) in anhydrous THF was added dropwise into the ice-cooled system and the reaction mixture was stirred in an ice bath for 4 h and another 48 h at room temperature under the protection of argon. After filtration, the solvent was removed by rotary evaporation, followed by re-dissolving the crude products in dichloromethane. The final products were isolated by precipitation in diethyl ether and dried under vacuum (yield: 64%). Bi(mPEG-PLGA)–*o*-PC and Bi(mPEG-PLGA)–*p*-PC were synthesized by the same procedure.

Nuclear magnetic resonance (NMR)

^1H NMR spectra were recorded with a 400 MHz proton NMR spectrometer (AVANCE III HD, Bruker) using $CDCl_3$ as the solvent and tetramethylsilane (TMS) as the internal standard. A 500 MHz proton NMR spectrometer (AVANCE III HD, Bruker) was used for ^{13}C NMR measurements with D_2O and DMSO-d_6 as the solvents. Chemical shift was referenced to the solvent in DMSO-d_6 (39.52 ppm for DMSO-d_6) and 4,4-dimethyl-4-silapentane-1-sulfonic acid sodium salt (DSS) as the internal standard in D_2O. The sample was equilibrated at the required temperature for 20 min before measurements.

Gel permeation chromatography (GPC)

The MWs and molar-mass dispersity ($Đ_M$) of copolymers were determined by using a gel permeation chromatography system (Agilent 1260) equipped with a refractive index detector. Measurements were performed at 35 °C with THF as the eluting solvent at a flow rate of 1.0 mL min^{-1}. The MWs were calibrated with the monodispersed polystyrene standards.

GPC–multi-angle light scattering (MALS)–viscometer (VIS) (GPC–MALS–VIS)

The absolute MW, intrinsic viscosity ($[\eta]$) and the Mark–Houwink parameters (α and K) of the synthesized copolymers were measured by GPC coupled with a multi-angle light scattering (MALS) detector (DAWN HELEOS II, Wyatt) as well as a viscometer (VIS) detector (ViscoStar, Wyatt) (GPC–MALS–VIS). THF was selected as the eluting solvent at a flow rate of 1.0 mL min^{-1} at 35 °C. The refractive index increment, dn/dc, representing the slope of the dependence of the refractive index (n) of a polymer solution as a function of the polymer concentration (c), was measured using a refractive index detector (OPTILAB T-rEX, Wyatt). The MALS detector was equipped with a laser at 658 nm and 18 multi-angle detectors. To ensure sufficient light scattering signals for acquiring convincing results, the concentrations of copolymers in THF were about 5 wt% for the GPC–MALS–VIS test.

Sol–gel transition

The sol–gel transition temperature was determined *via* the test tube inverting method.[39] Polymers were dissolved in distilled water and equilibrated at 4 °C overnight. Then, the 2 mL vials containing polymer solutions (25 wt%) were immersed in a water bath at a designed temperature for 15 min to reach equilibrium, followed by inverting 180°. The sample was regarded as a gel if no visual flow was observed within 30 s. The temperature was increased by 1 °C per step.

A dynamic stress-controlled rheometer (Kinexus, Malvern) was also used to investigate the sol–gel transition of polymer aqueous solutions (25 wt%) using a cone plate (diameter: 60 mm, cone angle: 1°). The fringe of the cone plate was overlaid with a thin layer of low-viscosity silicone oil to minimize the evaporation of solvent. Data were recorded at an oscillatory frequency ω of 10 rad s^{-1} and a heating rate of 0.5 °C min^{-1}.

Critical micelle concentration (CMC)

The CMC of the copolymer aqueous solutions was determined by the hydrophobic dye solubilization method.[45] The stock solution of 1,6-diphenyl-1,3,5-hexatriene (DPH) (50 μL, 0.4 mM in methanol) was injected into polymer aqueous solutions (5 mL) with concentrations ranging from 0.001 to 1.0 wt% and stored overnight at 4 °C. After equilibrating at 20 °C in the dark for 3 h, the absorption spectra of samples were recorded in the range from 300 to 450 nm using a UV-Vis spectrophotometer (TU-1950, PERSEE). The difference in absorbance between 377 and 400 nm ($A_{377} - A_{400}$) was plotted against the logarithmic polymer concentration. The data were fitted by using a Boltzmann fitting expressed as follows:

$$y = \frac{A_1 - A_2}{1 + \exp[(x - x_c)/d]} + A_2 \quad (1)$$

where y is the absorbance difference ($A_{377} - A_{400}$), x is the logarithm of the polymer concentration, A_1 and A_2 represent the asymptotic values of y at infinitely small and large x, x_c is the value at the center of the Boltzmann sigmoid, and d measures the deviation of x around x_c, respectively. The first turning point with respect to the low copolymer concentration is

 This journal is © The Royal Society of Chemistry 2017

Published on 13 March 2017. Downloaded by Fudan University on 11/11/2017 01:43:32.

defined as the CMC value. Alternatively, the CMC value could be obtained using the following equation:

$$\lg \mathrm{CMC} = x_c - 2d \quad (2)$$

Dynamic light scattering (DLS)

Hydrodynamic diameters of micelles were measured by DLS at a scattering angle of 90° (Zetasizer Nano, ZS 90, Malvern) as a function of temperature. Before measurements, polymer solutions (1 wt%) were filtered through a 0.45 μm filter to remove dust and equilibrated at each temperature for 15 min. Hydrodynamic diameters of particles were calculated following the Stokes–Einstein equation. The intensity–intensity time correction function was analyzed by the CONTIN method.

Transmission electron microscopy (TEM)

One drop of the polymer aqueous solution (1 wt%) was put on a copper grid coated with a superthin carbon film and then dried under an infrared lamp. Samples were observed under a transmission electron microscope (Tecnai G2 20 TWIN, FEI) with an accelerating voltage of 200 kV.

Monte Carlo simulation

Dynamic Monte Carlo simulation was used to model a single self-avoiding chain.[46,47] Since the lattice model had difficulties in simulating a polymer backbone with changing bond angles, the free rotation single chain conformation of Bi(mPEG-PLGA)–PC copolymers was studied by using a non-lattice model using the Monte Carlo method.[48] For simplicity, the athermal condition was applied and only the copolymer backbone chain was taken into account, *i.e.*, steric hindrance was considered the most important factor in the system. All atoms of the backbone chain were processed as beads. For the convenience of simulation, the benzene ring of PC was considered as a bead ignoring its spatial structure. The length between the bead representing the benzene ring and the bead linked to it was set at 2, while the lengths of other bonds in the backbone chain were set at the same constant value of 1.

The bond angles were set as follows: 120° for the carbonyl group; 60° for *o*-PC, 120° for *m*-PC and 180° for *p*-PC in the middle of the backbone; 109.5° for all other single bonds. All the coordinates of the atoms in the backbone chain could be calculated with the first atom set as the original point, and the second atom set as (1, 0, 0) and the rotation angle was determined by a random number between 0 and 2π. Under the above assumptions, the characteristic spatial conformational parameters could be obtained by the simulation.

Results

Synthesis and characterization of Bi(mPEG-PLGA)–*o*-PC, Bi(mPEG-PLGA)–*m*-PC and Bi(mPEG-PLGA)–*p*-PC

The mPEG-PLGA diblock copolymer was synthesized *via* a typical ring-opening polymerization of LA and GA in the presence of mPEG as the macroinitiator and $Sn(Oct)_2$ as the catalyst. The resulting diblock copolymer was further coupled using different coupling agents to produce the desired BAB-type triblock copolymers, as illustrated in Scheme 1. In this study, the conventional BAB-type triblock copolymer using HMDI as the coupling agent (usually specified as mPEG-PLGA-mPEG) was named Bi(mPEG-PLGA)–HMDI to highlight the role of the coupling agent. Correspondingly, the other three triblock copolymers obtained from the various isomers of phthaloyl dichloride (*o*-PC, *m*-PC and *p*-PC) were named Bi(mPEG-PLGA)–*o*-PC, Bi(mPEG-PLGA)–*m*-PC and Bi(mPEG-PLGA)–*p*-PC, respectively.

The ^{1}H NMR spectra of the mPEG-PLGA diblock copolymer and the corresponding triblock copolymers are shown in Fig. 2. The proton signal peaks appearing at 3.38 ppm (CH_3O– of mPEG, peak a), 4.80 ppm (–CH_2COO– of GA, peak d) and 5.20 ppm (–$CH(CH_3)COO$– of LA, peak e) were used for the determination of the number-average MW of the mPEG-PLGA diblock copolymer.[49] The other three characteristic peaks (f, b and c) at 1.55, 3.60 and 4.31 ppm were assigned to the methyl protons of LA units, PEG units and the methylene protons of PEG neighboring the PLGA block, respectively. The triblock copolymer Bi(mPEG-PLGA)–HMDI showed a spectrum similar to that of mPEG-PLGA except for the appearance of new proton peaks of HMDI moiety at 1.33 and 3.17 ppm (peaks g and h). For the Bi(mPEG-PLGA)–*p*-PC triblock copolymer, the characteristic phenyl proton signals just appeared at 8.15 ppm (peak i). In the case of Bi(mPEG-PLGA)–*m*-PC and Bi(mPEG-PLGA)–*o*-PC, the peaks at 7.57, 8.30 and 8.76 ppm (peaks j, k and l) were assigned to the phenyl proton signals of *m*-PC, while the peaks at 7.58 and 7.85 ppm (peaks m and n) belonged to the phenyl proton signals of *o*-PC. The integral ratio between the phenyl proton peaks of PC and the methoxy peak of mPEG was approximately in agreement with the theoretical stoichiometric ratio (4 : 3) for all the three samples.

Table 1 summarizes the molecular parameters of polymers synthesized in this study. All the BAB-type triblock copolymers possessed similar total MWs and LA/GA ratios based on the ^{1}H NMR measurements. These results provided evidence of the successful introduction of different coupling agents into

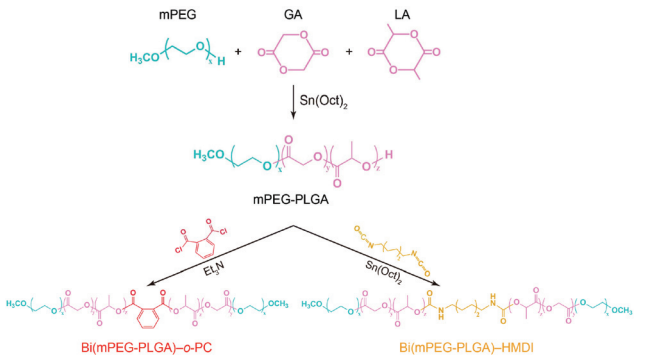

Scheme 1 Synthetic routes to mPEG-PLGA diblock copolymer and the corresponding triblock copolymers with *o*-PC and HMDI as the coupling agents.

Published on 13 March 2017. Downloaded by Fudan University on 11/11/2017 01:43:32.

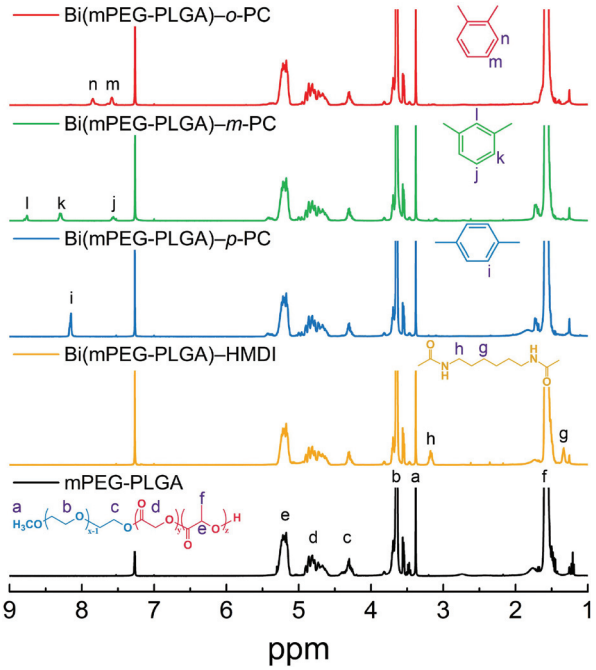

Fig. 2 ^{1}H NMR spectra of the mPEG-PLGA diblock copolymer and the indicated triblock copolymers using different coupling agents in $CDCl_3$.

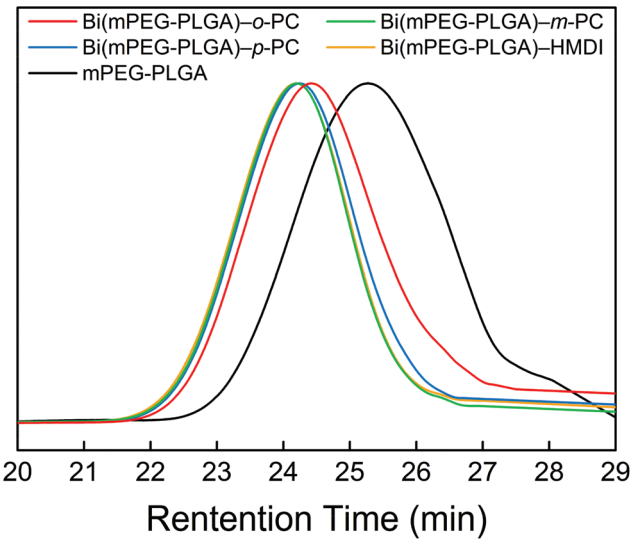

Fig. 3 GPC traces of the mPEG-PLGA diblock copolymer and the corresponding triblock copolymers obtained from different coupling agents.

the BAB-type triblock copolymers with a high conjugation efficiency.

The obtained specimens were further analyzed by GPC measurements and the results are presented in Fig. 3. All GPC traces of the diblock copolymer and triblock copolymers displayed a unimodal distribution. Compared with the original mPEG-PLGA diblock copolymer, the triblock copolymers held less retention time, indicating significantly increased MWs. Table 1 shows that the MWs of Bi(mPEG-PLGA)–*m*-PC and Bi(mPEG-PLGA)–*p*-PC were similar to that of conventional Bi(mPEG-PLGA)–HMDI and almost two times that of mPEG-PLGA. Also, their MW distributions reduced correspondingly after the coupling reaction compared with the initial mPEG-PLGA. These features demonstrated that the desired products were successfully synthesized.[50]

However, the MW of Bi(mPEG-PLGA)–*o*-PC was almost 1000 g mol^{-1} smaller than those of the other three triblock copolymers. Such a finding seems contradictory to the NMR results. Subsequently, the synthesis of Bi(mPEG-PLGA)–*o*-PC was repeated, whereas a similar GPC result was observed (data not shown).

Actually, the MW obtained from GPC analysis just reflects the size or hydrodynamic volume of the analyzed sample. Lower MW means smaller size or hydrodynamic volume of the polymer in the solvent. The three Bi(mPEG-PLGA)–PC triblock copolymers synthesized by us have the same molecular composition and the only difference lies in the spatial conformation of PC, as illustrated in Fig. 1B. *o*-PC as the coupling agent has a linking angle of 60°, while the linking angle of *m*-PC is 120° and that of *p*-PC increases to 180°. Hence, we infer that the smaller linking angle of Bi(mPEG-PLGA)–*o*-PC in the middle makes mPEG-PLGA chains closer to each other, resulting in a smaller coil size in the solvent. As a result, a relatively low MW was detected during the GPC analysis.

To verify this hypothesis, the absolute MW, the intrinsic viscosity ([η]) and the Mark–Houwink parameters (α and K) of the synthesized copolymers were also determined by GPC–MALS–VIS using THF as the solvent. The MW (M_w), hydrodynamic

Table 1 Parameters of the copolymers investigated in this study

Sample	M_n[a] (g mol^{-1})	LA/GA[a] (mol mol^{-1})	M_n[b] (g mol^{-1})	$Đ_M$[b]	Sol–gel transition temperature[c]
mPEG-PLGA	550-1350	2.9	2420	1.36	27 °C
Bi(mPEG-PLGA)–HMDI	550-1510-170-1510-550	2.8	5030	1.25	33 °C
Bi(mPEG-PLGA)–*o*-PC	550-1560-132-1560-550	2.8	3950	1.31	23 °C
Bi(mPEG-PLGA)–*m*-PC	550-1550-132-1550-550	2.9	5000	1.25	26 °C
Bi(mPEG-PLGA)–*p*-PC	550-1530-132-1530-550	2.8	4840	1.25	27 °C

[a] The number-average MW (M_n) of mPEG was provided by Aldrich. The M_n of each PLGA block and the molar ratio of lactide/glycolide (LA/GA) were calculated *via* ^{1}H NMR. [b] Determined by GPC using THF as an eluent relative to polystyrene standards. [c] Determined *via* the test tube inverting method. The polymer concentration was 25 wt% in water.

 This journal is © The Royal Society of Chemistry 2017

Published on 13 March 2017. Downloaded by Fudan University on 11/11/2017 01:43:32.

Table 2 Parameters of the copolymers obtained by GPC–MALS–VIS

Sample	dn/dc[a] (mL g^{-1})	M_w (g mol^{-1})	$Đ_M$	R_H[b] (nm)	K (mL g^{-1})	α	$[\eta]$[b] (mL g^{-1})
mPEG-PLGA	0.0522	2440	1.27	1.19	0.0511	0.59	4.68
Bi(mPEG-PLGA)–HMDI	0.0607	4430	1.08	1.74	0.0160	0.74	7.70
Bi(mPEG-PLGA)–*o*-PC	0.0586	4220	1.21	1.59	0.0380	0.62	6.48
Bi(mPEG-PLGA)–*m*-PC	0.0636	4110	1.16	1.72	0.0422	0.64	8.26
Bi(mPEG-PLGA)–*p*-PC	0.0612	4280	1.16	1.73	0.0184	0.73	8.03

[a] dn/dc was measured by a refractive index detector as shown in Fig. S1 of the ESI. [b] Data were presented as the weight average.

radius (R_H), and $[\eta]$ are presented as weight averages as recommended by the manufacturer for more convincing results. Table 2 clearly shows that the MW of Bi(mPEG-PLGA)–*o*-PC is similar to those of the other three specimens. This finding is well consistent with the NMR results. The R_H, α and $[\eta]$ of Bi(mPEG-PLGA)–*o*-PC were the smallest among the three triblock copolymers coupled with different PC isomers, suggesting that Bi(mPEG-PLGA)–*o*-PC surely has a smaller coil size. Such a compact structure is responsible for the lower MW in the GPC measurements.

Monte Carlo simulation of the spatial conformation of single Bi(mPEG-PLGA)–PC polymer chains

Monte Carlo simulation was further carried out to confirm the conformational difference among the three Bi(mPEG-PLGA)–PC triblock copolymers. We collected the statistics of the mean-squared end-to-end distance $\langle h^2 \rangle$, mean-squared radius of gyration $\langle R_g^2 \rangle$ and mean-squared distance between two side blocks $\langle D_{Centroid}^2 \rangle$ defined as the average of the squared distance between the centroids of the two segments linked by the middle coupling agent. Their distributions are shown in Fig. S2 of the ESI.†

Besides, the shape of each polymer chain was described based on the principal components $L_1^2 \leq L_2^2 \leq L_3^2$, the orthogonal components of $R_g^2 = L_1^2 + L_2^2 + L_3^2$ taken along the principal axes of inertia.[51,52] The parameter characteristic of the shape of molecules can be written as[52,53]

$$\langle \delta^* \rangle = 1 - 3\left\langle \frac{L_1^2 L_2^2 + L_2^2 L_3^2 + L_3^2 L_1^2}{(L_1^2 + L_2^2 + L_3^2)^2} \right\rangle \quad (3)$$

where $\langle \delta^* \rangle$ varies between 0 (sphere) and 1 (rod).

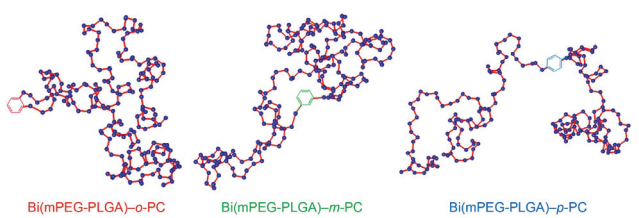

Fig. 4 Representative snapshots of the chains of Bi(mPEG-PLGA)–*o*-PC, Bi(mPEG-PLGA)–*m*-PC and Bi(mPEG-PLGA)–*p*-PC. The blue dots and read sticks represent the atoms and bonds, respectively. For brevity, all the hydrogen atoms and oxygen atoms of carbonyl groups are omitted.

Representative snapshots of the molecular spatial conformation of the three polymers are shown in Fig. 4. The simulation results summarized in Table 3 illustrate that Bi(mPEG-PLGA)–*o*-PC had the smallest $\langle h^2 \rangle$, $\langle R_g^2 \rangle$, $\langle D_{Centroid}^2 \rangle$ and $\langle \delta^* \rangle$. These features demonstrate that the coil of Bi(mPEG-PLGA)–*o*-PC is smaller than those of Bi(mPEG-PLGA)–*m*-PC and Bi(mPEG-PLGA)–*p*-PC, which is in agreement with the GPC–MALS–VIS results.

Macroscopic thermogelling behavior of concentrated polymer aqueous systems

All the polymers were soluble in water at ambient temperature and exhibited reversible sol–gel transitions as the temperature increased, as displayed in Fig. 1A. With further increase of temperature, the polymer aqueous systems underwent gel–precipitate transitions. The coupling agents had a significant influence on the sol–gel transition temperature. As shown in Table 1, the sol–gel transition temperature of the conventional Bi(mPEG-PLGA)–HMDI triblock copolymer in water (25 wt%), which was determined by the test-tube inverting method, shifted to a higher temperature after the coupling reaction compared with the original mPEG-PLGA diblock copolymer. This feature is consistent with our previous publications and others.[49,54–56] However, the Bi(mPEG-PLGA)–PC/water systems exhibited lower sol–gel transition temperatures when compared to Bi(mPEG-PLGA)–HMDI. In the case of Bi(mPEG-PLGA)–*m*-PC and Bi(mPEG-PLGA)–*p*-PC in water (25 wt%), the sol–gel transition temperature was 26 °C and 27 °C, respectively. The thermal-induced gelation transition temperature of Bi(mPEG-PLGA)–*o*-PC further decreased to 23 °C at the same concentration.

Dynamic rheology analysis was also performed to monitor the sol–gel transition of copolymer aqueous solutions as a function of temperature, and the results are shown in Fig. 5. The storage modulus G' and loss modulus G'' represent the load-bearing capacity and energy dissipating capacity under a cyclic deformation, respectively. All the polymer solutions were free-flowing with low G' (less than 0.01 Pa) at low temperatures, indicating their good injectability. As the temperature increased, an abrupt increase in both G' and G'' was observed for all the tested samples.

In general, the temperature at which G' is equal to G'' is defined as the sol–gel transition temperature.[57,58] The transition temperature determined by the rheology measurements is well consistent with that obtained from the test tube invert-

Published on 13 March 2017. Downloaded by Fudan University on 11/11/2017 01:43:32.

Table 3 Simulation results for triblock copolymers coupled with different isomers of PC[a]

Sample	$\langle h^2 \rangle$	$\langle R_g^2 \rangle$	$\langle D_{Centroid}^2 \rangle$	L_1^2	L_2^2	L_3^2	$\langle \delta^* \rangle$
Bi(mPEG-PLGA)–*o*-PC	424	72.3	151	4.4	12.2	55.7	0.44
Bi(mPEG-PLGA)–*m*-PC	439	75.8	165	4.5	12.5	58.8	0.45
Bi(mPEG-PLGA)–*p*-PC	457	80.0	182	4.6	12.9	62.5	0.46

[a] Results are presented as the average of 100 000 single polymer chains randomly selected for each group.

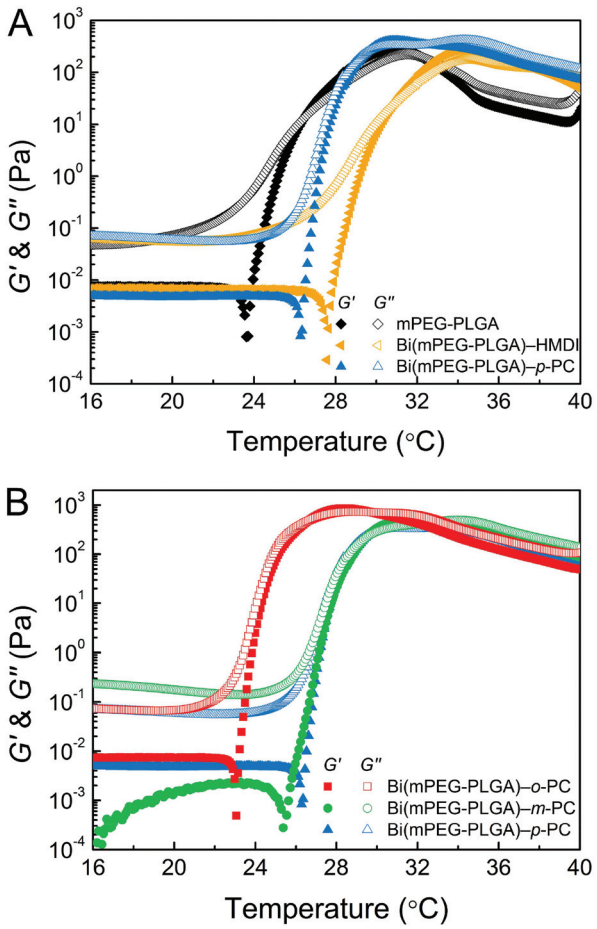

Fig. 5 Storage modulus G' and loss modulus G'' of (A) mPEG-PLGA, Bi(mPEG-PLGA)–HMDI, and Bi(mPEG-PLGA)–*p*-PC and (B) Bi(mPEG-PLGA)–*o*-PC, Bi(mPEG-PLGA)–*m*-PC, and Bi(mPEG-PLGA)–*p*-PC in water as a function of temperature. The polymer concentration was 25 wt%.

ing method, as shown in Table 1. The maximum storage modulus (G'_{max}) reflects the strength of the hydrogel. Compared with the original diblock copolymer mPEG-PLGA, the G'_{max} of Bi(mPEG-PLGA)–HMDI remained almost unchanged (270 *versus* 280 Pa). The value of G'_{max} increased to 480 Pa and 410 Pa after replacing HMDI with *m*-PC and *p*-PC, respectively. The increased rigidity of coupling agents might be responsible for the increased modulus. Interestingly, the G'_{max} of Bi(mPEG-PLGA)–*o*-PC was almost two times as large as those of Bi(mPEG-PLGA)–*m*-PC and Bi(mPEG-PLGA)–*p*-PC and reached 860 Pa.

Mesoscopic self-assembly of amphiphilic copolymers in water

It is well known that amphiphilic copolymers easily self-assemble into micelles in aqueous medium.[32–34] In this study, the micellization of the different samples in water was first monitored by a hydrophobic dye method using DPH as the probe. DPH has a higher UV-Vis absorbance in a hydrophobic environment than that in an aqueous environment. In general, DPH enters the hydrophobic cores preferentially with the formation of micelles, resulting in an increased absorption at 320–400 nm as a characteristic triplet band (Fig. 6A). The crossing point of the extrapolation of $A_{377} - A_{400}$ against logarithmic polymer concentration was defined as CMC. The absorbance at 400 nm was subtracted to eliminate the baseline effect as the concentration increased. To avoid subjectivity, the data were fitted by the Boltzmann fitting and then the CMC value was determined based on the acquired information on $x_c - 2d$ (eqn (2)), as shown in Fig. 6B and S3 of the ESI.†

The fitting parameters are listed in detail in Table S1 of the ESI.† While the CMC of the BA-type diblock copolymer was much lower than those of the BAB-type triblock copolymers, the CMC values did not present significant difference among the triblock copolymers, regardless of the type of coupling agent, as demonstrated in Fig. 6C and Table S1 (ESI†). This finding indicates that these BAB-type triblock copolymers have a similar ability to form micelles.

DLS measurements were utilized to determine the *Z*-averaging hydrodynamic diameter (D_h) of micelles in aqueous medium. As shown in Fig. 7A, the average micellar sizes of triblock copolymers coupled with *o*-PC, *m*-PC and *p*-PC were 48, 46 and 39 nm at 25 °C, respectively. The spherical morphology of micelles was further confirmed by TEM observation, as displayed in Fig. 7B. The micellar sizes obtained from TEM imaging coincided well with the DLS results. Besides, the micellar size distribution of Bi(mPEG-PLGA)–*o*-PC presented in Fig. 7B was more uniform than those of the other two samples. This feature is also consistent with the lower distribution of D_h of Bi(mPEG-PLGA)–*o*-PC in the DLS results.

The micellar behavior was further monitored with increasing temperature, as presented in Fig. 8. The average micellar sizes of Bi(mPEG-PLGA)–*m*-PC and Bi(mPEG-PLGA)–*p*-PC were maintained at around 40 nm until 40 °C and then increased abruptly, reflecting the aggregation of micelles. As to the Bi(mPEG-PLGA)–

 This journal is © The Royal Society of Chemistry 2017

Published on 13 March 2017. Downloaded by Fudan University on 11/11/2017 01:43:32.

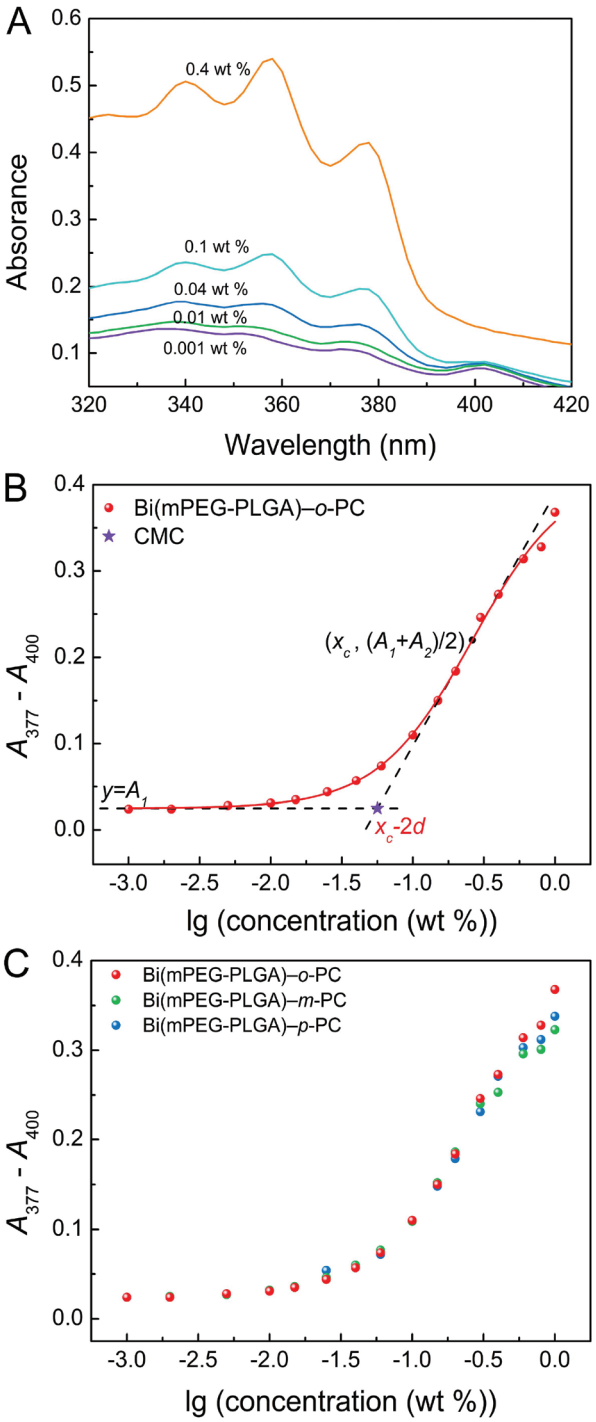

Fig. 6 (A) UV-Vis spectra of Bi(mPEG-PLGA)–*o*-PC aqueous solutions as a function of polymer concentration containing 4 μM DPH. The measurement temperature was 20 °C. For clarity, just five mass concentrations are displayed. (B) CMC determination of Bi(mPEG-PLGA)–*o*-PC aqueous solution by fitting the data with a Boltzmann sigmoid. Fitting parameters are listed in Table S1 of the ESI† and CMC was obtained by the crossing point. (C) The difference in absorbance between 377 and 400 nm for the indicated samples as a function of the copolymer concentration at 20 °C.

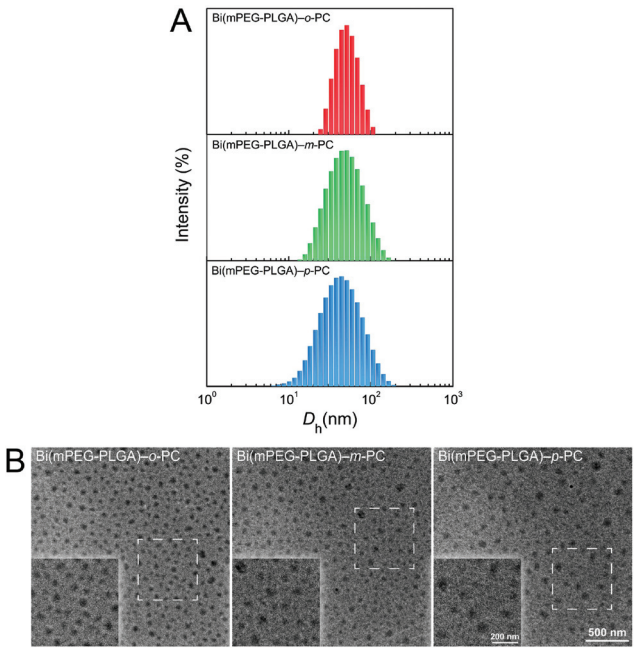

Fig. 7 (A) Distribution of hydrodynamic diameters D_h of micelles of the indicated copolymers in water at 25 °C. (B) TEM images showing the formation of micelles of the indicated copolymers. The inset pictures are the magnified images of the indicated regions. The polymer concentration was 1 wt%.

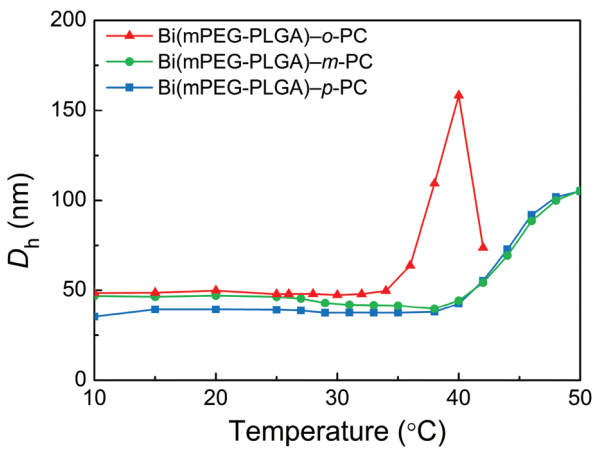

Fig. 8 Hydrodynamic diameter variation of micelles of the indicated copolymers in aqueous medium (1 wt%) as a function of temperature.

o-PC system, the temperature of micellar aggregation decreased to 36 °C. Also, at a higher temperature (42 °C), the average size of micellar aggregation decreased again, which might be attributed to the partial dehydration of the PEG segments.[59,60]

The change in the molecular environment of Bi(mPEG-PLGA)–*o*-PC copolymers upon heating was also detected by ^{13}C NMR. The ^{13}C NMR spectra of 25 wt% Bi(mPEG-PLGA)–*o*-PC in D_2O at the indicated temperatures are presented in Fig. 9A. Meanwhile, the ^{13}C NMR spectrum of Bi(mPEG-PLGA)–*o*-PC in PLGA (16.5 ppm) and the ethylene

Published on 13 March 2017. Downloaded by Fudan University on 11/11/2017 01:43:32.

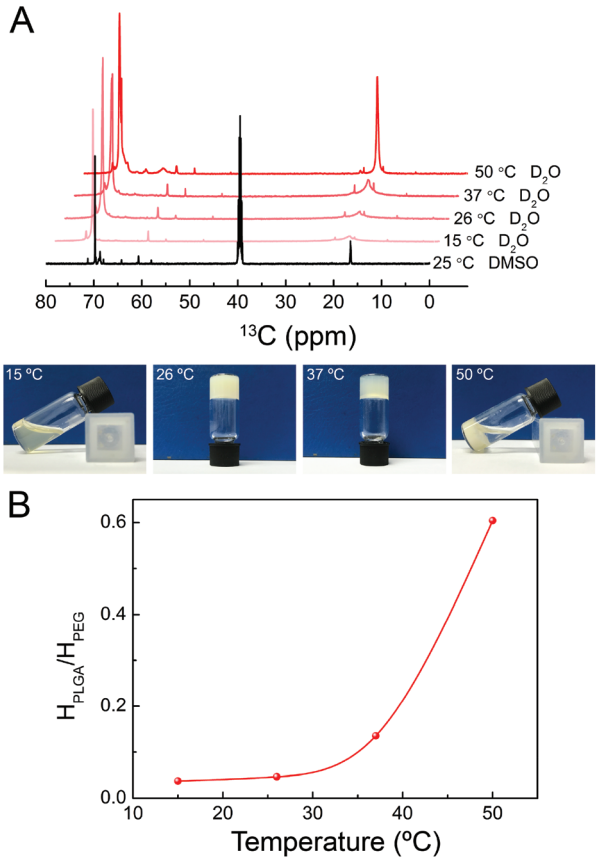

Fig. 9 (A) (Upper) ^{13}C NMR spectra of 25 wt% Bi(mPEG-PLGA)–*o*-PC in D_2O as a function of temperature. The spectrum in DMSO-d_6 is shown as the control. (Bottom) Optical images of Bi(mPEG-PLGA)–*o*-PC aqueous solution (25 wt%) exhibiting sol, gel and precipitate states at the indicated temperatures. (B) Peak height ratio of methyl (PLGA) to ethylene (PEG) in the ^{13}C NMR spectra of Bi(mPEG-PLGA)–*o*-PC as a function of temperature.

group of PEG (69.8 ppm) presented sharp peaks in DMSO-d_6 since DMSO is a good solvent for all the blocks of Bi(mPEG-PLGA)–*o*-PC. In contrast, water is a poor solvent for the PLGA block and a relatively good solvent for PEG. In the sol state (15 °C), the sharp peak of the ethylene group of PEG at 72–73 ppm and the collapsed peak of the methyl group of PLGA at 18–19 ppm indicate the formation of micelles with PLGA as cores and PEG as coronas in water. These characteristics basically remained unchanged in the gel state (26 °C, a temperature slightly above the sol–gel transition, and 37 °C, body temperature), suggesting that no abrupt change in the micellar structure occurred. The peak height ratio of PLGA to PEG gives a rough estimate of the molecular motion of polymers at each temperature (Fig. 9B). The low peak ratio in the sol and gel states reflects the intact micellar structure. At a higher temperature of 50 °C, the PEG peak was slightly broadened, whereas the peak height of the methyl group of PLGA increased pronouncedly. Also, the peak height ratio increased significantly, suggesting the destruction of the core–shell micellar structure, and a macroscopic precipitation was observed.

Discussion

Linear BAB-type (*e.g.*, mPEG-PLGA-mPEG) and ABA-type (*e.g.*, PLGA-PEG-PLGA) triblock copolymers constitute the two main branches of the family of thermogelling PEG/polyester polymers. Previous works have revealed that a small change of the end group could surprisingly affect the thermal gelation of ABA-type polymer aqueous solutions.[32,39–42] Hence, it is of interest to understand how the spatial conformation of the linkers in the middle of the BAB-type PEG/polyester polymers relates to their micro- or macroscopic aqueous behaviors. In a previous study, Cohn's group developed reverse thermo-responsive poly(ethylene oxide)–poly(propylene oxide) multiblock polymers with varied PC isomers as chain extenders.[61] They concluded that the structure of chain extenders played a key role in determining the sol–gel transition. The synthetic process of random multiblock poly(ether-ester)s was less controllable and thus the resulting polymers inevitably exhibited different MWs and molecular compositions. These diversities between polymers obscure the accurate reason for this interesting finding. More recently, Jeong's group reported a temperature/light dual-sensitive copolymer by coupling thermosensitive poly(ethylene glycol)-poly(L-alanine) with an azobenzene moiety.[57] The reversible *trans–cis* configurational change of the middle azobenzene group upon exposure to UV and visible light was able to remarkably influence the microscopic and macroscopic properties of the polymer aqueous solution. As they claimed, the conformational change of azobenzene also brings about the polarity change of azobenzene,[57] and thus it is difficult to distinguish the influence of spatial conformation and polarity in such a system. In the present work, three positional isomers of PC containing two functional groups at different spatial orientations were selected as the coupling agents and a systematic study of the positional isomeric effects of coupling agents on the thermogelling properties of the BAB-type PEG/polyester polymers was performed, and other interferential factors, such as MW and composition difference, were excluded on the basis of our molecular design.

^{1}H NMR and GPC–MALS–VIS measurements (Tables 1, 2 and Fig. 2) clearly confirmed that all three Bi(mPEG-PLGA)–PC triblock copolymers coupled *via* the positional isomers of PC had the same chemical composition and very similar MWs. This ensures the subsequent analysis of the spatial conformation and physicochemical properties of polymers. Interestingly, compared with the other two specimens, Bi(mPEG-PLGA)–*o*-PC presents a relatively smaller hydrodynamic volume in THF, a good solvent of the polymers, as reflected by a relatively lower MW during GPC analysis (Table 1 and Fig. 3). This feature was further verified by the GPC–MALS–VIS measurements as well as the Monte Carlo simulation (Tables 2 and 3). The relatively smaller coil of Bi(mPEG-PLGA)–*o*-PC was attributed to the 60° (<90°) linking angle of the *o*-PC isomer, which affects the spatial conformation of polymers.

All the BAB-type PEG/PLGA polymers underwent sol–gel transitions in water as the temperature increased. The

 This journal is © The Royal Society of Chemistry 2017

Published on 13 March 2017. Downloaded by Fudan University on 11/11/2017 01:43:32.

Bi(mPEG-PLGA)–PC/water systems showed lower sol–gel transition temperatures than the conventional Bi(mPEG-PLGA)–HMDI polymer (Table 1 and Fig. 5). The rigidity of the aromatic ring in the middle might be responsible for such a finding. There was no significant difference in sol–gel transition temperature and gel modulus between Bi(mPEG-PLGA)–*m*-PC and Bi(mPEG-PLGA)–*p*-PC. In contrast, a lower transition temperature and a higher gel modulus were observed in the case of Bi(mPEG-PLGA)–*o*-PC. For the three Bi(mPEG-PLGA)–PC systems, the only difference lies in the linking angle in the middle coupling position of each polymer chain (60° linkage of *o*-PC, 120° linkage of *m*-PC and 180° linkage of *p*-PC). Therefore, the difference was attributed to the positional isomeric effect of the coupling agents.

Next, their self-assembly behavior in water was examined and compared. We demonstrated that triblock copolymers containing different positional isomers of PC in the middle of polymers exhibited similar CMCs in water (Fig. 6C and Table S1 of the ESI†), indicating their similar ability to form micelles. A similar micellar size was also observed for the three polymer systems, whereas the temperature of micellar aggregation of the Bi(mPEG-PLGA)–*o*-PC system decreased to 36 °C when compared to the 40 °C of Bi(mPEG-PLGA)–*m*-PC and Bi(mPEG-PLGA)–*p*-PC systems. The 4 °C difference in the aggregation temperature between Bi(mPEG-PLGA)–*o*-PC and the other two Bi(mPEG-PLGA)–PC copolymers was quite in agreement with their sol–gel temperature difference, as demonstrated in Table 1 and Fig. 5B. Therefore, although the three Bi(mPEG-PLGA)–PC samples possessed similar capabilities for the formation of micelles, their different capabilities for micellar aggregation resulted in the change in the sol–gel transition temperatures for their concentrated polymer solutions.

The formation of a percolated micelle network through micellar aggregation has been put forward to interpret the sol–gel transition of thermogelling ABA-type PEG/polyester polymers in water.[32–34,45] We believe that the thermogelation of the current BAB-type system can also be explained by such a mechanism. Firstly, micelles with hydrophilic PEG as coronas and hydrophobic PLGA as cores are formed above CMC by the self-assembly of amphiphilic polymer chains in water (Fig. 6 and 7) and the CMC is much lower than the critical gel concentration (data not shown). Secondly, as the temperature increases, the hydrophobic interaction between micelles gives rise to the micellar aggregation, as demonstrated in Fig. 8. At a critical temperature, the hydrophobic interaction is sufficiently strong to induce the formation of a percolated network of micelles, resulting in the sol–gel transition (Fig. 5). Meanwhile, the intact micellar structure is maintained in the gel states, as displayed in Fig. 9. Finally, the micellar structure is broken due to the overly amplified hydrophobicity of copolymers at the higher temperature (Fig. 9), as reflected by the precipitate of polymers in water.

Finally, the positional isomeric effects on the sol–gel transition of Bi(mPEG-PLGA)–PC systems are schematically displayed in Fig. 10. The hydrophobic segments (PLGA and PC parts) of amphiphilic molecules tend to aggregate to decrease the exposed surface in the aqueous environment. Thus, the core–corona micellar structure was formed at a specific polymer concentration, namely CMC. This process was driven dominantly by the entropy change of the surrounding water molecules,[32,43] so there is no significant difference in CMC among the triblock copolymers coupled by various positional isomers of PC (Fig. 6C and Table S1 of the ESI†). However, the architecture of micellar cores may be different due to the various spatial conformations of the molecular chains of Bi(mPEG-PLGA)–PC polymers. The results of GPC, GPC–MALS–VIS and Monte Carlo simulation have confirmed that Bi(mPEG-PLGA)–*o*-PC has a smaller coil due to the 60° linkage of *o*-PC compared with Bi(mPEG-PLGA)–*m*-PC and

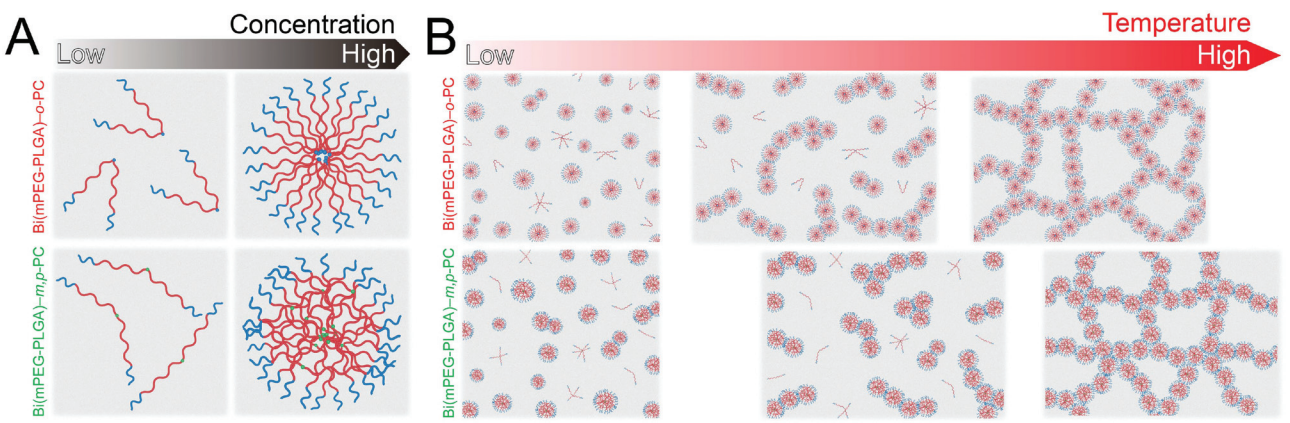

Fig. 10 Schematic representation of the sol–gel transition of the aqueous solutions of the block copolymers coupled with different positional isomers. (A) The formation of micelles in the aqueous solution as the concentration of polymers increases. The micelles of Bi(mPEG-PLGA)–*o*-PC have relatively more ordered cores than those of Bi(mPEG-PLGA)–*m*,*p*-PC. (B) The micellar aggregation and the formation of a percolated micelle network as the temperature increases. The micellar aggregation as well as the formation of a relatively stronger percolated micelle network happen at a lower temperature for Bi(mPEG-PLGA)–*o*-PC than that for Bi(mPEG-PLGA)–*m*,*p*-PC.

Published on 13 March 2017. Downloaded by Fudan University on 11/11/2017 01:43:32.

Bi(mPEG-PLGA)–*p*-PC systems (Tables 2 and 3, Fig. 4 and S2 of the ESI†). It is reasonable to suppose that the more spread conformation of the molecular chains of Bi(mPEG-PLGA)–*m*-PC and Bi(mPEG-PLGA)–*p*-PC leads to more chances to entangle with each other when the molecular chains self-assemble into the core–corona micelles, as illustrated in Fig. 10A. In contrast, the molecular chains of Bi(mPEG-PLGA)–*o*-PC have fewer opportunities to entangle with each other because of the relatively smaller coil, contributing to a comparatively regular core structure. As the temperature increases, the micelles start to aggregate driven by the hydrophobic interaction, as shown in Fig. 10B. This difference in the structure of micellar cores may result in two consequences for the macroscopic properties of polymer solutions, as reflected in the rheology tests (Fig. 5B). One is that the Bi(mPEG-PLGA)–*o*-PC micelles aggregate at lower temperature (Fig. 8), and thus a lower sol–gel transition temperature was observed. The other result is that the relatively ordered core phases of micelles of Bi(mPEG-PLGA)–*o*-PC could also interact with each other to a stronger extent after the aggregation of micelles as the temperature increases. The stronger interaction between micelles leads to the formation of a stronger percolated micelle network following the sol–gel transition, which might be the reason for the higher gel modulus of Bi(mPEG-PLGA)–*o*-PC.

Conclusions

This work reveals the positional isomeric effects of coupling agents on the microscopic and macroscopic properties of BAB-type triblock copolymer aqueous solutions. A series of BAB-type mPEG-PLGA-mPEG triblock copolymers with very similar chemical compositions and total MWs were synthesized by coupling mPEG-PLGA diblock copolymers with various linking moieties. All the triblock copolymers were soluble in aqueous medium and spontaneously turned into semi-solid hydrogels with an increase of temperature. After replacing the conventional coupling agent of HMDI with positional isomers of PC, the sol–gel transition temperatures of Bi(mPEG-PLGA)–PC polymers in water decreased while their gel moduli increased correspondingly. Also, the Bi(mPEG-PLGA)–*o*-PC/water system exhibited a lower thermal gelation temperature and a higher gel modulus than the copolymers linking with *m*-PC and *p*-PC isomers. The sol–gel transition of such a system was attributed to the formation of a percolated micelle network with increasing temperature. Compared with the other two samples, Bi(mPEG-PLGA)–*o*-PC itself has a smaller coil due to the 60° linkage of *o*-PC. This different spatial conformation seems to be responsible for the increased tendency for micellar aggregation of the Bi(mPEG-PLGA)–*o*-PC system upon heating, which resulted in a reduced thermal gelation temperature and an increased gel modulus in spite of the lack of significant difference in the CMCs or micellar sizes among the three specimens. This research not only enriches the strategy to modulate the sol–gel transition of thermogelling polymers but also may afford new ideas to design other functional biomaterials and devices.

Acknowledgements

The work was supported by the National Natural Science Foundation of China (grant no. 21474019 and 51273217), the State Key Project of Research and Development (grant no. 2016YFC1100300), and the Science and Technology Developing Foundation of Shanghai (grant no. 14441901500 and 15JC1490300).

Notes and references

1 M. A. C. Stuart, W. T. S. Huck, J. Genzer, M. Muller, C. Ober, M. Stamm, G. B. Sukhorukov, I. Szleifer, V. V. Tsukruk, M. Urban, F. Winnik, S. Zauscher, I. Luzinov and S. Minko, *Nat. Mater.*, 2010, **9**, 101–113.
2 Q. V. Nguyen, J. S. Lym, C. T. Huynh, B. S. Kim, H. J. Jae, Y. I. Kim and D. S. Lee, *Polym. Chem.*, 2016, **7**, 5805–5818.
3 C. Hu, F. Tian, Y. Zheng, C. S. Y. Tan, K. R. West and O. A. Scherman, *Chem. Sci.*, 2015, **6**, 5303–5310.
4 W. Xiong, X. H. Fu, Y. M. Wan, Y. L. Sun, Z. B. Li and H. Lu, *Polym. Chem.*, 2016, **7**, 6375–6382.
5 S. X. Li, L. Liu, L. J. Zhang, B. Wu, C. X. Wang, W. Zhou, R. X. Zhuo and S. W. Huang, *Polym. Chem.*, 2016, **7**, 5113–5122.
6 M. Tong, X. N. An, W. D. Pan, H. H. Liu and Y. L. Zhao, *Polym. Chem.*, 2016, **7**, 2209–2221.
7 W. D. Pan, H. H. Liu, H. C. Zhang and Y. L. Zhao, *Polym. Chem.*, 2016, **7**, 2870–2881.
8 J. F. Quinn, M. R. Whittaker and T. P. Davis, *Polym. Chem.*, 2017, **8**, 97–126.
9 H. J. Moon, D. Y. Ko, M. H. Park, M. K. Joo and B. Jeong, *Chem. Soc. Rev.*, 2012, **41**, 4860–4883.
10 L. Yu and J. D. Ding, *Chem. Soc. Rev.*, 2008, **37**, 1473–1481.
11 A. Petit, B. Muller, R. Meijboom, P. Bruin, F. van de Manakker, M. Versluijs-Helder, L. G. J. de Leede, A. Doornbos, M. Landin, W. E. Hennink and T. Vermonden, *Biomacromolecules*, 2013, **14**, 3172–3182.
12 Z. X. Zhang, K. L. Liu and J. Li, *Angew. Chem., Int. Ed.*, 2013, **52**, 6180–6184.
13 G. Barouti, S. S. Liow, Q. Dou, H. Ye, C. Orione, S. M. Guillaume and X. J. Loh, *Chem. – Eur. J.*, 2016, **22**, 10501–10512.
14 M. Le Bohec, M. Banère, S. Piogé, S. Pascual, L. Benyahia and L. Fontaine, *Polym. Chem.*, 2016, **7**, 6834–6842.
15 T. Vermonden, R. Censi and W. E. Hennink, *Chem. Rev.*, 2012, **112**, 2853–2888.
16 L. Zhang, W. J. Shen, J. B. Luan, D. X. Yang, G. Wei, L. Yu, W. Y. Lu and J. D. Ding, *Acta Biomater.*, 2015, **23**, 271–281.
17 Y. P. Chen, Y. Z. Li, W. J. Shen, K. Li, L. Yu, Q. H. Chen and J. D. Ding, *Sci. Rep.*, 2016, **6**, 31593.
18 M. Patel, H. J. Moon, D. Y. Ko and B. Jeong, *ACS Appl. Mater. Interfaces*, 2016, **8**, 5160–5169.
19 D. Y. Kim, D. Y. Kwon, J. S. Kwon, J. H. Kim, B. H. Min and M. S. Kim, *Polym. Rev.*, 2015, **55**, 407–452.

 This journal is © The Royal Society of Chemistry 2017

Published on 13 March 2017. Downloaded by Fudan University on 11/11/2017 01:43:32.

20 J. Y. Lin, P. L. Lai, Y. K. Lin, S. Peng, L. Y. Lee, C. N. Chen and I. M. Chu, *Polym. Chem.*, 2016, **7**, 2976–2985.
21 L. Chen, X. Q. Li, L. P. Cao, X. L. Li, J. R. Meng, J. Dong, L. Yu and J. D. Ding, *Chin. J. Polym. Sci.*, 2016, **34**, 147–163.
22 Z. Zhang, J. Ni, L. Chen, L. Yu, J. W. Xu and J. D. Ding, *Biomaterials*, 2011, **32**, 4725–4736.
23 K. Shi, Y. L. Wang, Y. Qu, J. F. Liao, B. Y. Chu, H. P. Zhang, F. Luo and Z. Y. Qian, *Sci. Rep.*, 2016, **6**, 19077.
24 L. P. Cao, Q. L. Li, C. Zhang, H. C. Wu, L. Q. Yao, M. D. Xu, L. Yu and J. D. Ding, *ACS Biomater. Sci. Eng.*, 2016, **2**, 393–402.
25 H. J. Moon, M. Patel, H. Chung and B. Jeong, *Adv. Healthcare Mater.*, 2016, **5**, 353–363.
26 J. Park, I. Y. Kim, M. Patel, H. J. Moon, S.-J. Hwang and B. Jeong, *Adv. Funct. Mater.*, 2015, **25**, 2573–2582.
27 M. H. Park, Y. Yu, H. J. Moon, D. Y. Ko, H. S. Kim, H. Lee, K. H. Ryu and B. Jeong, *Adv. Healthcare Mater.*, 2014, **3**, 1782–1791.
28 K. W. Lei, W. J. Shen, L. P. Cao, L. Yu and J. D. Ding, *Chem. Commun.*, 2015, **51**, 6080–6083.
29 Y. M. Kim, C. H. Kim and S. C. Song, *ACS Macro Lett.*, 2016, **5**, 297–300.
30 B. B. Seo, H. Choi, J. T. Koh and S. C. Song, *J. Controlled Release*, 2015, **209**, 67–76.
31 M. S. Shim, H. T. Lee, W. S. Shim, I. Park, H. Lee, T. Chang, S. W. Kim and D. S. Lee, *J. Biomed. Mater. Res.*, 2002, **61**, 188–196.
32 L. Yu, G. T. Chang, H. Zhang and J. D. Ding, *J. Polym. Sci., Part A: Polym. Chem.*, 2007, **45**, 1122–1133.
33 L. Chen, T. Y. Ci, T. Li, L. Yu and J. D. Ding, *Macromolecules*, 2014, **47**, 5895–5903.
34 L. Chen, T. Y. Ci, L. Yu and J. D. Ding, *Macromolecules*, 2015, **48**, 3662–3671.
35 L. Yu, H. T. Hu, L. Chen, X. G. Bao, Y. Z. Li, L. Chen, G. H. Xu, X. J. Ye and J. D. Ding, *Biomater. Sci.*, 2014, **2**, 1100–1109.
36 Y. P. Chen, J. B. Luan, W. J. Shen, K. W. Lei, L. Yu and J. D. Ding, *ACS Appl. Mater. Interfaces*, 2016, **8**, 30703–30713.
37 Y. M. Chung, K. L. Simmons, A. Gutowska and B. Jeong, *Biomacromolecules*, 2002, **3**, 511–516.
38 S. J. Bae, J. M. Suh, Y. S. Sohn, Y. H. Bae, S. W. Kim and B. Jeong, *Macromolecules*, 2005, **38**, 5260–5265.
39 L. Yu, H. Zhang and J. D. Ding, *Angew. Chem., Int. Ed.*, 2006, **45**, 2232–2235.
40 A. Petit, B. Muller, P. Bruin, R. Meyboom, M. Piest, L. M. J. Kroon-Batenburg, L. G. J. de Leede, W. E. Hennink and T. Vermonden, *Acta Biomater.*, 2012, **8**, 4260–4267.
41 S. Jo, J. Kim and S. W. Kim, *Macromol. Biosci.*, 2006, **6**, 923–928.
42 J. Y. Kim, M. H. Park, M. K. Joo, S. Y. Lee and B. Jeong, *Macromolecules*, 2009, **42**, 3147–3151.
43 B. Jeong, Y. H. Bae and S. W. Kim, *Colloids Surf., B*, 1999, **16**, 185–193.
44 C. Y. Gong, S. Shi, P. W. Dong, B. Kan, M. L. Gou, X. H. Wang, X. Y. Li, F. Luo, X. Zhao, Y. Q. Wei and Z. Y. Qian, *Int. J. Pharm.*, 2009, **365**, 89–99.
45 T. Li, T. Y. Ci, L. Chen, L. Yu and J. D. Ding, *Polym. Chem.*, 2014, **5**, 979–991.
46 G. Q. Xu, J. D. Ding and Y. L. Yang, *J. Chem. Phys.*, 1997, **107**, 4070–4084.
47 W. Q. Lu and J. D. Ding, *Macromolecules*, 2006, **39**, 7433–7440.
48 Y. L. Yang and H. D. Zhang, *Monte Carlo Method in Polymer Science (in Chinese)*, Fudan University Press, Shanghai, 1993.
49 K. T. Peng, C. F. Chen, I. M. Chu, Y. M. Li, W. H. Hsu, R. W. Hsu and P. J. Chang, *Biomaterials*, 2010, **31**, 5227–5236.
50 N. A. Lynd, A. J. Meuler and M. A. Hillmyer, *Prog. Polym. Sci.*, 2008, **33**, 875–893.
51 K. Solc and W. H. Stockmay, *J. Chem. Phys.*, 1971, **54**, 2756–2757.
52 G. Zifferer and W. Preusser, *Macromol. Theory Simul.*, 2001, **10**, 397–407.
53 O. Jagodzinski, E. Eisenriegler and K. Kremer, *J. Phys. I*, 1992, **2**, 2243–2279.
54 J. B. Luan, W. J. Shen, C. Chen, K. W. Lei, L. Yu and J. D. Ding, *RSC Adv.*, 2015, **5**, 97975–97981.
55 W. J. Shen, J. B. Luan, L. P. Cao, J. Sun, L. Yu and J. D. Ding, *Biomacromolecules*, 2015, **16**, 105–115.
56 K. W. Kwon, M. J. Park, Y. H. Bae, H. D. Kim and K. Char, *Polymer*, 2002, **43**, 3353–3358.
57 S. Y. Jeong, H. J. Moon, M. H. Park, M. K. Joo and B. Jeong, *J. Polym. Sci., Part A: Polym. Chem.*, 2012, **50**, 3184–3191.
58 L. P. Cao, B. Cao, C. J. Lu, G. W. Wang, L. Yu and J. D. Ding, *J. Mater. Chem. B*, 2015, **3**, 1268–1280.
59 L. Yu, Z. Zhang and J. D. Ding, *Biomacromolecules*, 2011, **12**, 1290–1297.
60 S. Y. Kim, H. J. Kim, K. E. Lee, S. S. Han, Y. S. Sohn and B. Jeong, *Macromolecules*, 2007, **40**, 5519–5525.
61 A. Sosnik and D. Cohn, *Biomaterials*, 2005, **26**, 349–357.